



Research Article

## Strain Distribution for CP-Ti in Cyclic Extrusion Compression Angular Pressing by RSM

B. Pasoodeh<sup>1</sup>, V. Alimirzaloo<sup>1,\*</sup>, M. Shahbaz<sup>2</sup>, K. Hajizadeh<sup>3</sup> and J. Alizadeh Kaklar<sup>1</sup>

<sup>1</sup> Department of Mechanical Engineering, Faculty of Engineering, Urmia University, Urmia, Iran

<sup>2</sup> Department of Materials Science and Engineering, Faculty of Engineering, Urmia University, Urmia, Iran

<sup>3</sup> Faculty of Mining and Metallurgical Engineering, Urmia University of Technology, Urmia, Iran

### ARTICLE INFO

#### Article history:

Received 25 August 2023

Reviewed 11 November 2023

Revised 18 November 2023

Accepted 20 November 2023

#### Keywords:

Strain distribution

CECAP process

Response surface method

Finite element analysis

CP-Ti

#### Please cite this article as:

B. Pasoodeh, V. Alimirzaloo, M. Shahbaz, K. Hajizadeh, J. Alizadeh Kaklar, Strain Distribution for CP-Ti in Cyclic Extrusion Compression Angular Pressing by RSM, *Iranian Journal of Materials Forming*, 10(3) (2023) 25-35.

### ABSTRACT

Cyclic extrusion compression angular pressing (CECAP) is a novel severe plastic deformation (SPD) method applied to improve the mechanical and metallurgical properties of materials. In this research, finite element analysis and response surface method were considered for CP-Ti in CECAP process. Temperature, input extrusion diameter, exit extrusion angle, shear factor and longitudinal distance of input extrusion to the ECAP region were selected as input parameters to study strain distribution in the current process. The analysis of variance (ANOVA) was developed for current work, and the results showed that input parameters of input extrusion diameter and shear factor, and the interaction of the temperature and longitudinal distance of input extrusion to ECAP region, and the shear factor and longitudinal distance of input extrusion to ECAP region considerably affect the strain distribution. Hardness measurement in section A at the points near the center and outer surfaces of the sample showed the hardness of 21 and 24 HRC respectively. At this point, the maximum difference for hardness was achieved at about 12% throughout the cross section which is in suitable agreement with the strain distribution model. Moreover, the optical microscope (OM), both current CDECAP and conventional CECAP, showed that the majority of deformed grains were enlarged. The average deformed grain size for the current CECAP was reduced to 100 nm, which is considerably smaller than the conventional CECAP with an average grain size of 300 nm. Furthermore, the load-stroke diagram was achieved by executing experimental tests and comparing the results achieved the numerical model. The results showed a good agreement between them.

© Shiraz University, Shiraz, Iran, 2023

## 1. Introduction

Titanium and its alloys, e.g., Ti-6Al-4V have excellent properties such as corrosion behavior, mechanical properties and biocompatibility that is used

in the field of fabricating biomedical equipment which has received great attention among investigators [1,2]. Due to the wide advantages of nanostructured and ultrafine-grained materials by SPD methods, researchers have considerably used them. Many investigators have focused on the modification, improvement, and development of new SPD methods, because of its excellent advantages such as: improved mechanical

\* Corresponding author

E-mail address: [v.alimirzaloo@urmia.ac.ir](mailto:v.alimirzaloo@urmia.ac.ir) (V. Alimirzaloo)

<https://doi.org/10.22099/IJMF.2023.48186.1268>



characteristics and grain refinement [3, 4]. Although, titanium alloys such as Ti–6Al–4V have better mechanical properties compared to pure titanium (CP-Ti), there is a problem with this alloy releasing toxic metal ion by alloying elements and biological incompatibility restricting its application [5, 6]. Hence, CP-Ti is a suitable choice for medical purposes, provided that, the strength of it be improved by grain refinement. Under these circumstances, CECAP is one of those techniques that produces nanostructured materials [7-8].

To produce high plastic strain in materials, cyclic extrusion compression (CEC) is one of the well-known SPD techniques used. In the mentioned method, an initially cylindrical sample enters through two similar cylindrical channels (vertical to each other) with the same diameter linked via a reduced cross-section neck (extrusion). In each operation of the CEC process, it performs an extrusion followed by compression in the second channel helped by backpressure to retain its initial shape. However, in order to retain the initial shape, the backpressure should be applied for the reverse compression in the second channel of CEC noticed as the main problem with the current method. To solve this problem, a new technique, namely cyclic expansion extrusion (CEE), was introduced to eliminate the backpressure from the CEC process [9, 10]. In this technique, when the material touches the outlet channel, its movement is temporarily obstructed causing it to expand the material under pressure. But, the investigations showed that non-uniform material flow in the longitudinal section of the sample over the extrusion and expansion is the main problem with this method [11].

Equal channel angular pressing (ECAP) is an SPD method being widely used for severe plastic deformation demands. It has been used for a wide variety of materials such as Al-Mg alloys, AZ91 alloy, AZ31 alloy, and Titanium alloys [12]. In spite of having excellent properties of the ECAPed samples, the papers showed that strain inhomogeneity on the sample sections can be considered as the main problem of the current procedure [13,14]. In order to solve the problems of CEC and

ECAP methods, CECAP was developed combining advantage of CEC and ECAP methods by M. Ensafi et al. [15]. In the first step of the current method, the cylindrical sample goes through a compression extrusion (input) before reaching the ECAP region. Then, as the sample touches the ECAP section, due to the applied pressure by that area, the sample starts to fill the space between the CEC and ECAP areas resulting in the sample restoring its initial shape. The combination of the CEC and ECAP simultaneously shows its advantages on the CECAP. The accumulative applied strain that is achieved is equal to the total strains on CEC and ECAP methods. However, it suffers from lower hydrostatic compression stresses on the CECAPed samples that is identified as the problem of the current method. In order to solve the stated problem, S. Ahmadi et al. [7] proposed a novel CECAP method enhancing the hydrostatic compression stress and strain uniformity on CECAPed samples. In their method, an extrusion area was added to the horizontal (output) channel. Hence, the strain non-uniformity and the lack of hydrostatic compressive stress were compensated by the extra extrusion area. S. Ahmadi et al. [16] investigated the microstructure and the mechanical properties of the AM60 magnesium alloy by using the new CECAP method. Results showed that the proposed method and the CECAP-processed conditions created more hardness values to rise constantly, up to 196% and 175% for the proposed CECAP and conventional CECAP methods after four passes compared to the unprocessed samples, respectively.

Due to the lack of studies considering the effects of the process and geometrical parameters of the CECAP process for CP-Ti, this study has been conducted to indicate the influences of the input parameters including the temperature ( $T$ ), input extrusion diameter ( $D$ ), exit extrusion angle ( $\alpha$ ), shear factor ( $m$ ), and the longitudinal distance of input extrusion to the ECAP region ( $L$ ) on the respond parameter of strain distribution. For that reason, the response surface method (RSM) and FEM were selected. The Design of Expert and Deform 3-D software's were applied to run experiments and the simulations, respectively.

Furthermore, due to the lack of sufficient investigations carried out to analyze CP-Ti (with excellent medical applications) processed by CECAP with the mentioned input variables, it was decided to investigate this material as a case study. Moreover, a load-stroke diagram and microhardness measurement were performed to validate the accuracy of the FEM simulations. Moreover, ANOVA analysis was performed to calculate the significant parameters and to determine the accuracy of the proposed mathematical model.

## 2. Experimental Procedure

### 2.1. Principles of CECAP

In the CECAP process, two interchangeable extrusion inserts are located before and after the ECAP zone. The die was fabricated from two cylindrical channels with a diameter of 15 mm, and an ECAP deformation area consisting of a channel angle of 90° and a corner angle of 20°. As the operation starts, the input extrusion zone with a 2 mm reduction receives the cylindrical sample with a diameter of 15 mm passing through the vertical channel. Then, due to the resistance applied by the end of the vertical cylindrical channel (ECAP zone), it starts to expand and restore its initial shape (diameter 15 mm). In the next step, the sample goes through the ECAP area and receives more strains. Ultimately, the sample reaches the output extrusion zone at the end of the horizontal channel. This area forms a diameter reduction by 1 mm. Moreover, it creates an extra backpressure on the CECAP process. The sum of the strain applied to the sample on the CECAP process, is the combination of the three different operations including the ECAP and two extrusion stages denoted by Eqs. (1), (2) and (3) [7, 15, 16]. Thus, Eq. (4) can be used to present the total applied strain on the CECAP process for one pass:

$$\varepsilon_{ECAP} = 1 / \sqrt{3} \{2 \cot(\varphi / 2 + (\psi) / 2) + \psi \csc(\varphi / 2 + \psi / 2)\} \quad (1)$$

$$\varepsilon_{EXi} = 4 \ln M/D \quad (2)$$

$$\varepsilon_{EX0} = 2 \ln M/E \quad (3)$$

$$\varepsilon_{CECAP} = \{1 / \sqrt{3} [2 \cot(\varphi / 2 + \psi / 2) + \psi \csc(\varphi / 2 + \psi / 2)] + 4 \ln M / D + 2 \ln M / E\} \quad (4)$$

Where,  $\alpha_1$  and  $\alpha_2$  show the input and exit extrusion angles with values of 60°.  $\varphi$  and  $\psi$  depict the channel angle and corner angle on the CECAP die as illustrated in Fig. 1. The main vertical and horizontal channels diameter (namely M, D and E) represent the input and output extrusion diameters, respectively. As can be seen from Eq. (4), this relation is independent of the strain rate and the frictional coefficient. Thus, their influences will be considered separately.

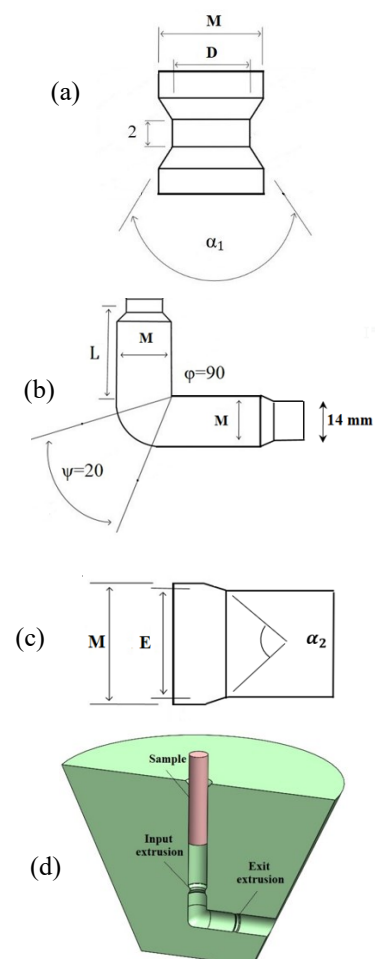


**Fig. 1.** (a) Input Extrusion zone (b) ECAP region (c) Exit Extrusion zone (d) CECAP model.

## 2.2. Materials and Method

In this paper, CP-Ti in the form of cold extruded rod was applied, the chemical composition of which is illustrated in Table 1. Samples with 15 mm in diameter and 70 mm in length were machined by a wire cut machine from the as-received CP-Ti rod. They were then annealed at 650 °C for 60 min by an electric furnace and then furnace-cooled to room temperature to improve their plastic deformation. To show the accuracy of the proposed numerical model, the hardness of the experimentally fabricated sample was measured and compared by numerical results. Rockwell C (HRC- ISO 6508-1) hardness measurements were executed in the current work. The tests were carried out on the cross-section perpendicular to the moving axis of the sample. As illustrated on Fig. 2 (c), the ceramic heater was applied to rise the sample temperature during operation. The temperature applied by this heater has a tolerance of 5 °C controlled by a laser heat measurement device (Taipo IRG 1350) as shown in Fig. 2 (b). Moreover, to enhance the accuracy of the performed tests, the indentation was repeated 5 times at each location on the sections and the average microhardness values were reported. A split CECAP die configuration consisting of two similar symmetric sets were applied Fig. 2. Hot compression test was performed at temperatures of 270 °C, 300 °C, and 330 °C [17] and the strain rates of 0.01, 0.1, and 1 s<sup>-1</sup> to extract the stress-strain behavior of the used CP-Ti in the current simulation. Finally, the stress-strain behavior of the mentioned material obtained from the experimental hot compressive tests were achieved as illustrated in Fig. 3. Using an optical microscope (OM), the microstructural observation for the as-received CP-Ti with an average grain size of 10 µm has been shown in Fig. 3 (d). For OM observation, the selected areas were polished with 0.05 µm colloidal silica and etched in a solution containing 2%HF+6%HNO<sub>3</sub>+92%H<sub>2</sub>O.

**Table 1.** Chemical composition of used CP-Ti in the current study

| Element                 | O    | N    | Fe   | Pd   | Mg   | Cr  |
|-------------------------|------|------|------|------|------|-----|
| Percentage<br>volume(%) | 0.19 | 0.03 | 0.14 | 0.19 | 0.12 | 0.2 |

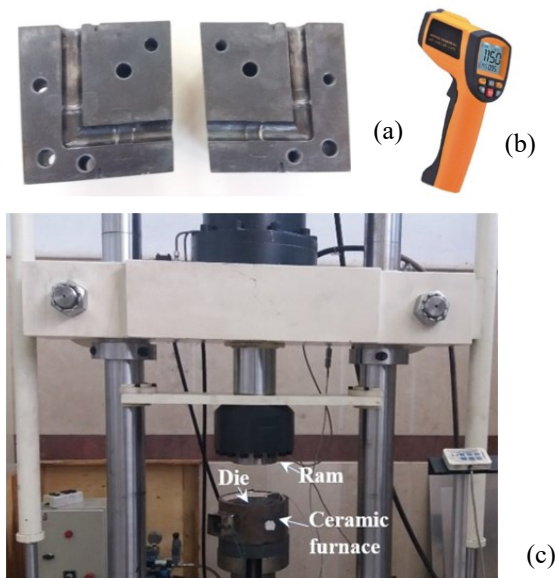


**Fig. 2.** (a) The current designed CECAP die set, (b) Laser heat measurement device and (c) Press applied for experimental process

## 2.3. Finite Element Method

The commercial Deform-3D V.11 software was applied to simulate the experiments in the current study. The sample was assumed to be plastic with a cylindrical shape of a diameter of 15 mm and a height of 70 mm. CECAP dies and rams were designed to be rigid bodies in the simulation process. The shear friction model was applied to simulations based on the values of reference [18]. The mesh convergence criterion was applied to determine the precise mesh numbers and then, tetrahedral element with a total number of 60000 was selected. The automatic remeshing option was activated to accommodate large deformation over simulation.

## 2.4. Response Surface Methodology (RSM)

Proper selection of the input process and die parameters in the CECAP process have a significant effect on the quality and improvement of CECAPed samples. Hence, the development of the relation among input and respond parameters can considerably affect the results. Design Expert V11 software was used to obtain the RSM central composite design (CCD) set of experiments with five input variables in three levels as illustrated in Table 2. The temperature, input extrusion diameter, exit extrusion angle, shear factor, and the

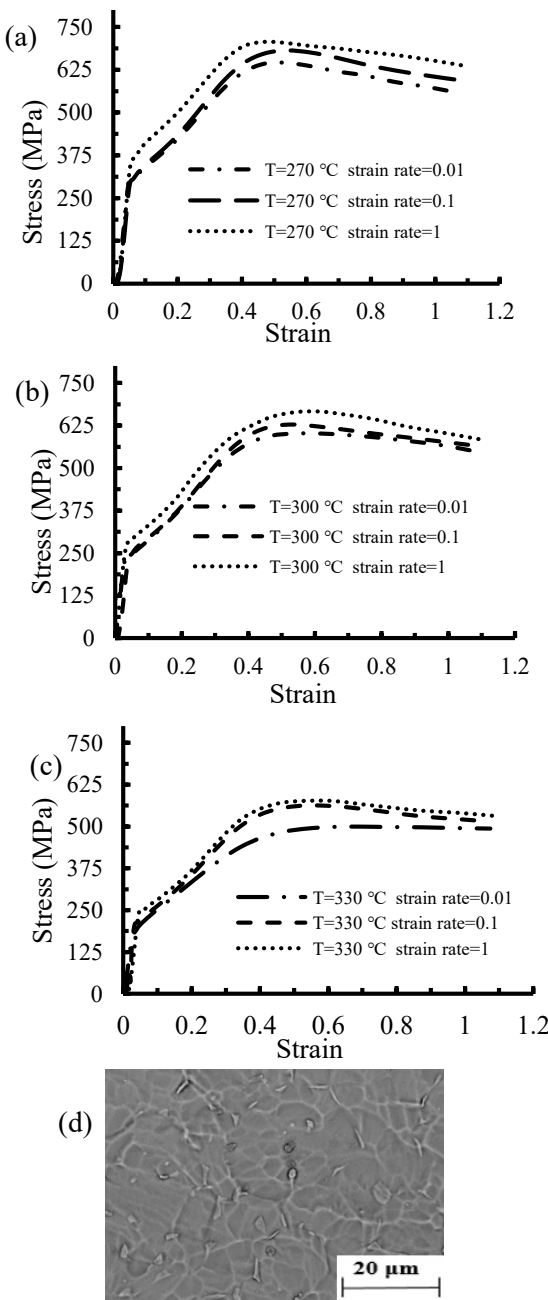


**Fig. 3.** Stress-strain behavior of CP-Ti obtained from the hot compression test for various temperatures and strain rates, (a) 270 °C , (b) 300 °C , and (c) 330 °C (d) Optical microscope of as-received CP-Ti used in the current paper.

longitudinal distance of input extrusion to the ECAP region were selected as input parameters, and the strain distribution was selected as the responding variable. A total of 30 experimental tests (24 separate experiments with 6 repetitions of the central point) were calculated, as shown in Table 3. To verify the effectiveness of the proposed mathematical model, ANOVA was executed. It was also used to determine the significant factors by calculating with a p-value lower than 0.05. Quantitative

equation, namely standard deviation (S.D), was applied and written by Eqs. (5) and (6) [19], as follows:

$$S.D = \sqrt{\frac{\sum_{i=1}^n (\varepsilon_i - \varepsilon_{ave})^2}{n}} \quad (5)$$

$$\varepsilon_{ave} = \frac{\sum_{i=1}^N (\varepsilon_i)}{N} \quad (6)$$

Where,  $\varepsilon_i$  and  $\varepsilon_{ave}$  represent the effective strain distribution at the  $i^{th}$  point and the average strain distribution. N is the number of the selected points on the cross section.

**Table 2.** Process parameters and their levels involved in the analysis

| Variables \ Level   | Index | Level 1 | Level 2 | Level 3 |
|---|-------|---------|---------|---------|
| Temperature ( $T$ , °C)   | A     | 270     | 300     | 330     |
| Input extrusion diameter (D, mm)                                | B     | 11      | 12      | 13      |
| Exit extrusion angle ( $\alpha$ , degree)                       | C     | 50      | 60      | 70      |
| Shear factor (m)  | D     | 0.3     | 0.5     | 0.7     |
| Longitudinal distance of input extrusion to ECAP region (L, mm) | E     | 12      | 15      | 18      |

### 3. Results and Discussion

ANOVA is implemented to inspect the accuracy and effectiveness of the proposed mathematical RSM-based model, and to determine significant factors, as illustrated in Table 4. In this investigation, the F value states whether the variance between the means of two population is significantly different or not, where, as the F value rises, the relative variance among the group means improves. The p-value shown by the ANOVA analysis is a significant criterion determining the significant parameters and their percentage contribution on respond, where, if p-value for an individual factor is calculated to be less than 0.05, the factor can be considered as significant. Finally, the results observed

from the p-value and F-value of the ANOVA table shows that among the CECAP input parameters, input

**Table 3.** Experimental design matrix and respond values for CECAP process for CP-Ti

| Experiment | Temperature (T) | Input extrusion diameter (D) | Exit angle ( $\alpha$ ) | Frictional coefficient (m) | Longitudinal distance of input extrusion to ECAP region | Standard deviation (strain distribution) (S.D) |
|------------|-----------------|------------------------------|-------------------------|----------------------------|---|--|
| 1          | 270             | 11                           | 50°                     | 0.3                        | 18  | 0.0490   |
| 2          | 330             | 11                           | 50°                     | 0.3                        | 12  | 0.0437   |
| 3          | 270             | 13                           | 50°                     | 0.3                        | 12  | 0.712  |
| 4          | 330             | 13                           | 50°                     | 0.3                        | 18  | 0.0386   |
| 5          | 270             | 11                           | 70°                     | 0.3                        | 12  | 0.0219   |
| 6          | 330             | 11                           | 70°                     | 0.3                        | 18  | 0.0357   |
| 7          | 270             | 13                           | 70°                     | 0.3                        | 18  | 0.0265   |
| 8          | 330             | 13                           | 70°                     | 0.3                        | 12  | 0.0354   |
| 9          | 270             | 11                           | 50°                     | 0.7                        | 12  | 0.0339   |
| 10         | 330             | 11                           | 50°                     | 0.7                        | 18  | 0.0422   |
| 11         | 270             | 13                           | 50°                     | 0.7                        | 18  | 0.0673   |
| 12         | 330             | 13                           | 50°                     | 0.7                        | 12  | 0.0853   |
| 13         | 270             | 11                           | 70°                     | 0.7                        | 18  | 0.0672   |
| 14         | 330             | 11                           | 70°                     | 0.7                        | 12  | 0.0426   |
| 15         | 270             | 13                           | 70°                     | 0.7                        | 12  | 0.0833   |
| 16         | 330             | 13                           | 70°                     | 0.7                        | 18  | 0.0596   |
| 17         | 270             | 12                           | 60°                     | 0.5                        | 15  | 0.0508   |
| 18         | 330             | 12                           | 60°                     | 0.5                        | 15  | 0.0456   |
| 19         | 300             | 11                           | 60°                     | 0.5                        | 15  | 0.0612   |
| 20         | 300             | 13                           | 60°                     | 0.5                        | 15  | 0.0432   |
| 21         | 300             | 12                           | 50°                     | 0.5                        | 15  | 0.0381   |
| 22         | 300             | 12                           | 70°                     | 0.5                        | 15  | 0.0273   |
| 23         | 300             | 12                           | 60°                     | 0.3                        | 15  | 0.0384   |
| 24         | 300             | 12                           | 60°                     | 0.7                        | 15  | 0.0442   |
| 25         | 300             | 12                           | 60°                     | 0.5                        | 12  | 0.0272   |
| 26         | 300             | 12                           | 60°                     | 0.5                        | 18  | 0.0102   |
| 27         | 300             | 12                           | 60°                     | 0.5                        | 15  | 0.0304   |
| 28         | 300             | 12                           | 60°                     | 0.5                        | 15  | 0.0304   |
| 29         | 300             | 12                           | 60°                     | 0.5                        | 15  | 0.0304   |
| 30         | 300             | 12                           | 60°                     | 0.5                        | 15  | 0.0304   |
| 31         | 300             | 12                           | 60°                     | 0.5                        | 15  | 0.0304   |
| 32         | 300             | 12                           | 60°                     | 0.5                        | 15  | 0.0304   |

**Table 4.** Analysis of Variance (ANOVA) of results for the CECAP process to identify significant factors

| Source          | DOF | Seq-SS   | Adj-SS   | Adj-MS   | F-value | P-value |
|-----------------|-----|----------|----------|----------|---------|---------|
| <b>Model</b>    | 20  | 0.006799 | 0.006799 | 0.00034  | 2.8     | 0.041   |
| A: (T)          | 1   | 0.000029 | 0.000029 | 0.000029 | 0.24    | 0.635   |
| B: (D)          | 1   | 0.000436 | 0.000436 | 0.000436 | 3.9     | 0.05    |
| C: ( $\alpha$ ) | 1   | 0.000059 | 0.000059 | 0.000059 | 0.48    | 0.501   |
| D: (m)          | 1   | 0.001049 | 0.001049 | 0.001049 | 8.66    | 0.013   |
| E: (L)          | 1   | 0.000228 | 0.000228 | 0.000228 | 1.88    | 0.198   |
| AB              | 1   | 0.000018 | 0.000018 | 0.000018 | 0.15    | 0.705   |
| AC              | 1   | 0.000011 | 0.000011 | 0.000011 | 0.09    | 0.765   |
| AD              | 1   | 0.000039 | 0.000039 | 0.000039 | 0.32    | 0.58    |
| AE              | 1   | 0.000774 | 0.000774 | 0.000774 | 6.39    | 0.028   |
| BC              | 1   | 0.000252 | 0.000252 | 0.000252 | 2.08    | 0.177   |
| BD              | 1   | 0.000799 | 0.000799 | 0.000799 | 6.6     | 0.026   |
| BE              | 1   | 0.000487 | 0.000487 | 0.000487 | 4.02    | 0.07    |
| CD              | 1   | 0.000105 | 0.000105 | 0.000105 | 0.86    | 0.373   |
| CE              | 1   | 0.000417 | 0.000417 | 0.000417 | 3.44    | 0.091   |
| DE              | 1   | 0.000766 | 0.000766 | 0.000766 | 6.32    | 0.029   |

extrusion diameter and shear factor, and the interaction of temperature and longitudinal distance of input extrusion to ECAP region, shear factor and longitudinal distance of input extrusion to ECAP region considerably affect the strain distribution, where the remaining parameters seem to be insignificant in the current analysis. Finally, the mathematical formulation between input parameters and standard deviation for strain distribution presented according to Eq. 7, are as follows:

*Standars Deviation (S.D)*

$$\begin{aligned}
 &= 0.03327 - 0.001095 A \\
 &- 0.004262 B - 0.001562 C \\
 &- 0.006612 D + 0.003079 E \\
 &+ 0.001068 AB - 8.4375 AC \\
 &+ 0.001568 AD + 0.006956 AE \\
 &- 0.003968 BC + 0.007068 BD \\
 &- 0.005518 BE + 0.002556 CD \\
 &- 0.005106 CE - 0.006918 DE
 \end{aligned} \quad (7)$$

Distribution of minimum, maximum and average strain values for current CECAP (test number 26 from Table 3 with lowest S.D value), conventional CECAP [15] and new CECAP [7] processes have been illustrated in Fig 4. It is seen that the current CECAP method better improves the strain values compared to the new CECAP [7] and the conventional CECAP [15] where, the maximum strain value has gone up to 4.2% and 10.2% with respect to the new CECAP [7] and conventional CECAP [15], respectively. Although, a significant improvement has been achieved for strain value in the current CECAP approach, the strain inhomogeneity seems to have more significantly improved in comparison to the maximum strain values. It also obtains a reduction of about 10.2% compared to the new CECAP [7]. Moreover, the comparison of the maximum and minimum effective strain difference ratio for various ram speeds ( $((\varepsilon_{max} - \varepsilon_{min})|_{V=0.2 \text{ mm/sec}} / (\varepsilon_{max} - \varepsilon_{min})|_{V=0.35 \text{ mm/sec}}$ ) in the case of the current optimized CECAP, the new CECAP [7] and the conventional CECAP [15] states that, its value for the current CECAP is lower than those two methods (Fig. 5). This is because of the use of optimal conditions for the process parameters which causes strain to be distributed uniformly and with higher values. Furthermore, it can be due to the velocity variations between material elements

and torsional deformation mode at the center and surface of the CECAPed sample and its effect on minimum strain at the center of sample [20]. Finally, the mathematical relation between input parameters and standard deviation for strain inhomogeneity are stated as follows:

$$\begin{aligned} \text{Standard Deviation for Strain Inhomogeneity} \\ = & 0.0145 + 0.0076 V + 0.0042 N \\ - & 0.0053 C + 0.0037 L \\ + & 0.0021 VN + 0.0083 VE \\ - & 0.0065 VL - 3.641 NE \\ - & 0.0087 NL + 0.0012 E \end{aligned} \quad (8)$$

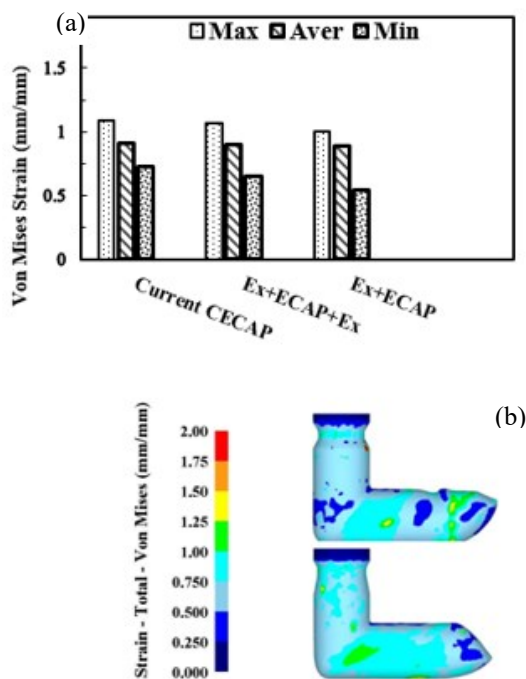


**Fig. 4.** (a) Mini, maxi and average strain values current CECAP, (Input extrusion+ECAP+Exit extrusion) [7], (Input extrusion+ECAP) [15] for  $V=0.2$  mm/s,  $\alpha = 60^\circ$ , 0.5, D=12 mm, L=18 mm,  $T = 300^\circ\text{C}$ . Simulation model for (b) current CECAP and (c) conventional CECAP [15].

In order to accurately figure out the strain distribution at various zones of the CECAPed specimen for the new CECAP [7] and current CECAP, the distribution of the effective strain at three different sections namely, A, B and C (three sections are the areas after input extrusion, after ECAP and after exit extrusion zones, respectively) were analyzed (Fig. 6). The Graph provided in Fig. 6 (a) shows that. In all three paths, the strain depicts inhomogeneity on the sections of the specimen for both methods. For path A, due to the presence of input

extrusion, the strain inhomogeneity seems to be intensive for both methods and the effective strain values increases to about 1.5. In this path, although, the effective strain value for the two methods has the same value, the strain distribution is better for the current CECAP method, where the maximum strain difference was calculated at about 0.9, while, for the new CECAP [7] it was 1.2. At path B, the sample passes through the ECAP area and the strain rises again causing inhomogeneity. Under these circumstances, due to the intense plastic strain mechanism at areas near the inner parts of the die, as shown in the diagram, the maximum effective strain for the new CECAP [7] reaches 2.9. however, the strain distribution behaves better for the current CECAP compared to the new CECAP [7]. Finally, at path C, as expected, because of the applied hydrostatic compressive stress, and consequently extra strain by exit extrusion operation, the strain inhomogeneity appeared for both methods. However, due to the use of the optimal parameters for the current CECAP process, the strain inhomogeneity has a better condition compared to the new CECAP [7]. Figs. 6 (b), (c) and (d) show the numerically CECAPed samples for the current CECAP process at three mentioned sections (A, B and C) and the effective strain and strain inhomogeneity are seen through the sections.

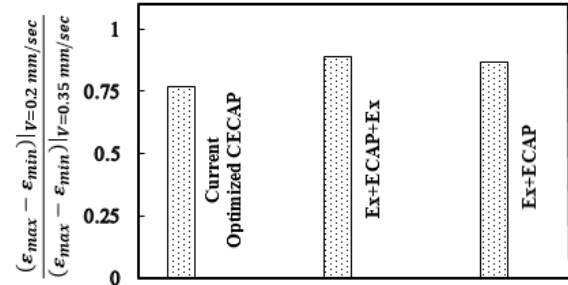
The experimental CECAPed samples of CP-Ti in the current CECAP process was carried out to verify the validity of the proposed numerical model, as illustrated in Fig. 7. For that reason, a load-stroke diagram for both experimental and numerical samples was obtained. Moreover, the hardness was measured for the current CECAP and new CECAP methods [7]. The measurements were performed on the cross sections perpendicular to the moving axis before and after the ECAP zone in the CECAP process, as illustrated on Fig. 7 (b). For further study, the hardness measurement in the HRC (Rockwell) scale in the longitudinal section parallel to the moving axis of the CECAPed sample was also measured as illustrated in Fig. 7 (c).

Fig. 8 compares the hardness distribution on the experimental samples between new CECAP [7] and current CECAP. At Fig. 8 (a) for current CECAP, the

hardness in section A at the points near the center and outer surfaces of the sample receive up to 21 and 24 HRC respectively, where, the maximum variation for hardness was calculated at about 12% throughout the cross section which is in good agreement with the distribution model of the strain distribution. The micro-hardness distribution in section B shows a steady fine downward trend dropping from the upper end of the sample to its lower end. At section C (after exit extrusion), the hardness distribution shows a behavior similar to the strain pattern, where, its maximum and minimum reaches the values of 31 and 28.7 HRC, respectively. Fig. 8 (a), showed that, the experimentally fabricated specimen for the current CECAP improves the strain inhomogeneity compared to the new CECAP by 3%, 5% and 8% at sections A, B and C, respectively. The pattern for hardness distribution can be related to the microstructural evolution and obtained plastic strain. For that reason, the Hall-Petch relationship [20] can be applied to show how the obtained hardness can be assigned to strain values. This relation proves that the hardness of materials strongly depends on the grain size [21], where, as strain intensity and consequently grain size decreases, the hardness rises with the same trend. Fig. 8 (b) shows the hardness distribution along the moving direction of the sample, where there are three increases along the path Q shown at Fig. 7 (c) relating to the input extrusion, ECAP and exit extrusion zones, respectively.

The experimentally fabricated CP-Ti sample in the current CECAP die has been shown in Fig. 7. As it was stated previously, it was used to investigate the validity and accuracy of the proposed numerical model. For that reason, the load-stroke curve of CECAP process was developed for both the experimental and numerical ones. The diagrams show three increases of slope over the stroke relating to input extrusion, ECAP and exit extrusion zones, respectively, as illustrated in Fig. 9. However, there is some difference between graphs, where in all domains, due to the presence of some impurities and microstructural defects in the tested material, the graph for the experimental method shows slightly more operation load. Fig. 10 illustrates OM of

CP-Ti after the CECAP process extracted from the transverse section depicting grain refinement. As expected, there is a significant refinement in grain size compared to as-received microstructure (Fig. 3 (d)).



**Fig. 5.** Comparison of the strain distribution ratio for different ram speeds [7, 15].

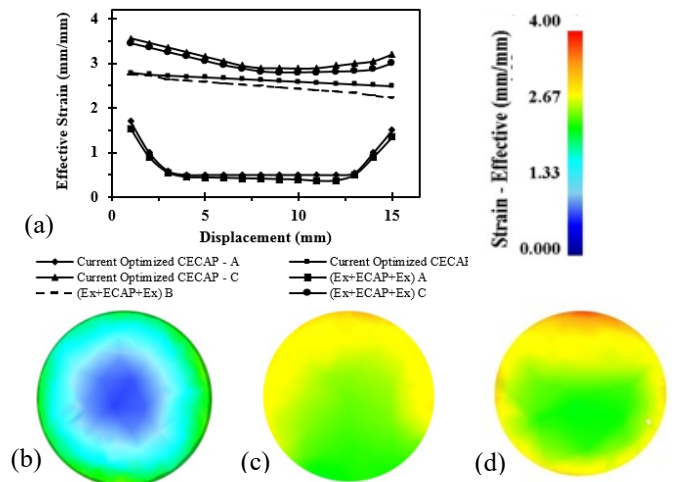


**Fig. 6.** (a) Effective strain achieved for new CECAP [7] and current optimized CECAP for various sections (b) Section A, (c) Section B and (d) Section C.

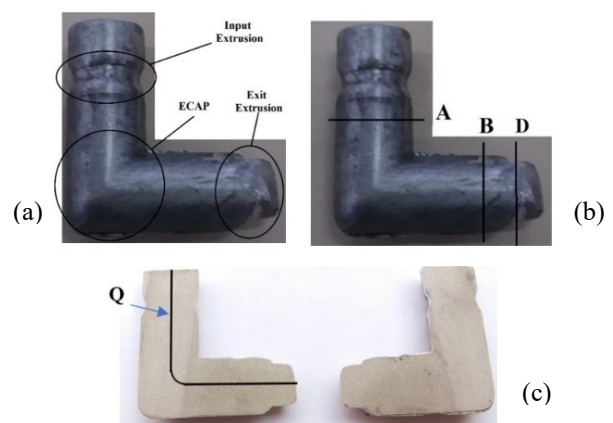


**Fig. 7.** (a) Experimental CECAPed CP-Ti sample (b) The cross sections used for hardness measurements (HRC) (c) Two splits of fabricated sample cut from longitudinal section parallel to moving axis.

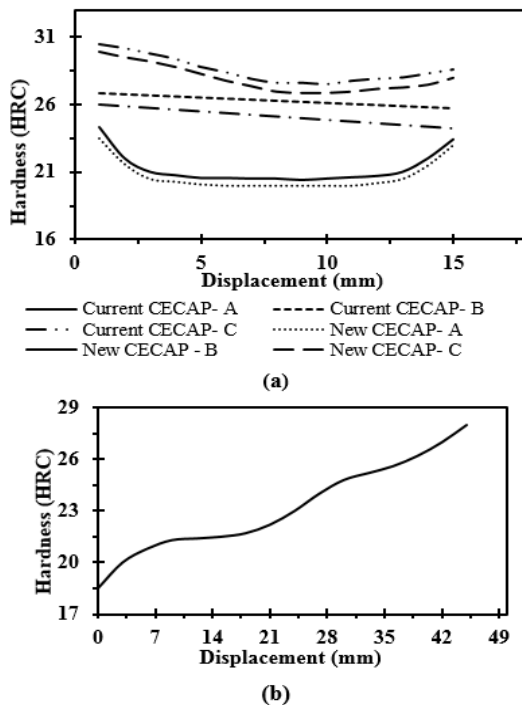


**Fig. 8.** (a) Hardness distribution achieved from experimental tests on the cross sections perpendicular to moving axis before and after ECAP zones, and after exit extrusion for current CECAP and new CECAP [7] (b) Hardness distribution along the longitudinal section parallel to moving axis (path Q) of CECAPed sample in the current CECAP process.

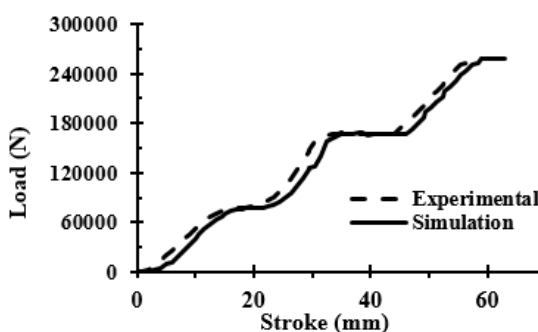


**Fig. 9.** The load-stroke diagram in the CECAP process for CP-Ti to compare the experimental and numerical methods.

A glance at the graph provided in Fig. 10, revealed that for both current CECAP and conventional CECAP [15], the majority of deformed grains were enlarged and very fine structure appeared. The average deformed grain size for current CECAP was reduced to 100 nm, which is smaller than for conventional CECAP with an average grain size of 300 nm. Comparison of Fig. 10 (a) and (b) disclosed that the microstructure of the current CECAP is significantly composed by grains seeming to be elongated less compared by conventional CECAP

method. Thus, it can be concluded that, although, there is a small quantitative difference in the strain inhomogeneity in OM observation between the mentioned methods, the elongation of the deformed grains for current CECAP along the moving axis seems to be less.

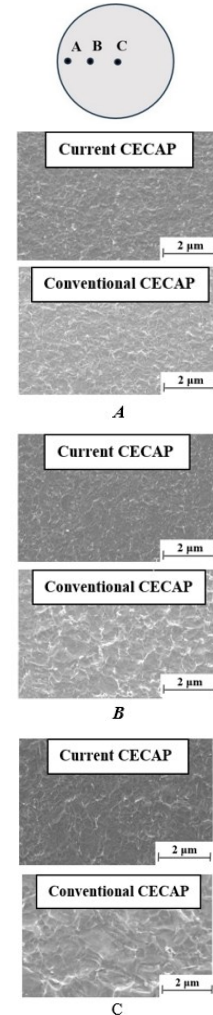


**Fig. 10.** OM observation for deformed CP-Ti extracted from transverse section (after exit extrusion zone) in the different positions A, B and C.

#### 4. Conclusion

CECAP was studied to inspect the influence of the input parameters including temperature, input extrusion diameter, exit extrusion angle, shear factor and longitudinal distance of input extrusion to the ECAP region on strain inhomogeneity (respond parameter). FEM and RSM were used to carry out the investigation. Medical importance of CP-Ti has motivated the authors to consider it as a case study. To quantify the strain

inhomogeneity, standard deviation was calculated. RSM and ANOVA were executed to mathematically develop the model for the response and calculate the effectiveness of the parameters, respectively. Deform 3-D and Design Expert software were employed to numerically simulate the process, and run the RSM experiments, respectively. Finally, the following conclusions can be drawn:

- Results revealed that input parameters of B (input extrusion diameter) and D (shear factor), and the interaction of AE (temperature and longitudinal distance of input extrusion to ECAP region) and DE (shear factor and longitude distance of input extrusion to ECAP region) significantly influence the strain distribution, where the remaining parameters seem to be insignificant variables in the current study.
- Comparison for hardness distribution on the experimental samples between the new CECAP [7] and the current CECAP were carried out. The results showed that the hardness in section A at the points near the center and outer surfaces of the sample obtained the hardness of 21 and 24 HRC respectively, which is in good agreement with the strain distribution pattern. Moreover, the results also showed that the experimental specimen for the current CECAP enhances the strain inhomogeneity compared to the new CECAP by 3%, 5% and 8% at sections A, B and C, respectively.
- The comparative investigation has been performed between the results of the numerical model and the experimental method for the CECAP process. The load-stroke diagram was carried out and the results showed a suitable agreement between their outcomes.
- Optical microscope analysis taken from the longitudinal section of the CECAPed samples for both the current and conventional CECAP methods were carried out and the results showed that the strain inhomogeneity has improved in the current proposed method. The average grain size of deformed sample for the current CECAP was

reduced to 100 nm, which is smaller than for conventional CECAP with an average grain size of 300 nm.

### **Acknowledgments**

The authors declare that they have no known competing financial interests or personal relationships that could have appeared to influence the work reported in this paper.

### **Conflict of Interests**

All authors state that there is no potential conflicts of interest when submitting this article.

### **5. References**

- [1] R. Valiev, Y. Estrin, Z. Horita, T. Langdon, M. Zehetbauer, Y. Zhu, Fundamentals of superior properties in bulk nanoSPD materials, *Materials Research Letters*, 4 (2016) 1-21.
- [2] W. Jiang, H. Cui, Y. Song, Electrochemical corrosion behaviors of titanium covered by various TiO<sub>2</sub> nanotube films in artificial saliva, *J. Mater. Sci.*, 53 (2018).
- [3] M. Kaur, K. Singh, Review on titanium and titanium-based alloys as biomaterials for orthopaedic applications, *Mater. Sci. Eng. C*, 102 (2019) 844-853.
- [4] Y. Chehrehsaz, K. Hajizadeh, A. Hajizadeh, L. Moradi, S. Mahshid, Effect of ECAP on Physicochemical and Biological Properties of TiO<sub>2</sub> Nanotubes Anodized on Commercially Pure Titanium, *Metals and Materials International*, 4 (2021) 67-78.
- [5] M. Aghaei. Khafri, N. Golarzi, Dynamic and metadyanamic recrystallization of hastelloy X superalloy, *journal of materials science*, 43 (2008) 3717-3724.
- [6] K. Indira, U.K. Mudali, T. Nishimura, N. Rajendran, A Review on TiO<sub>2</sub> Nanotubes: Influence of Anodization Parameters, Formation Mechanism, Properties, Corrosion Behavior, and Biomedical Applications, *J. Bio. Trib. Corros.*, 3 (2015) 1-28.
- [7] S. Ahmadi, V. Alimirzaloo, G. Faraji, A. Donyavi, A New Modified Cyclic Extrusion Channel Angular Pressing (CECAP) Process for Producing Ultrafine-Grained Mg Alloy, *Trans Indian Inst Met*, 73 (10) (2020) 2447-2456.
- [8] K. Hajizadeh, B. Eghbali, Effect of Two-Step Severe Plastic Deformation on the Microstructure and

- Mechanical Properties of Commercial Purity Titanium, *Met. Mater. Int.*, 20 (2014) 343-350.
- [9] M. W. Richert, Features of Cyclic Extrusion Compression: Method, Structure & Materials Properties, *Solid State Phenomena*, 114 (2006) 19-28.
- [10] N. Pardis, B. Talebanpour, R. Ebrahimi, S. Zomorodian, Cyclic expansion-extrusion (CEE): A modified counterpart of cyclic-compression (CEC), *Mater. Sci. Eng. A*, 528 (2011) 7537-7540.
- [11] S. Amani, G. Faraji, K. Abrinia, Microstructure and hardness inhomogeneity of fine grain AM60 magnesium alloy subjected to cyclic expansion extrusion (CEE), *Journal of Manufacturing Processes*, 28 (2017) 197-208.
- [12] M. Kawasaki, T. G. Langdon, Superplasticity in ultrafine-grained materials, *Rev. Adv. Mater. Sci.* 54 (2018) 46-55.
- [13] J. Zhang, K. S. Zhang, W. Hwai-Chung, M. H. Yu, Experimental and numerical investigation on pure aluminium by ECAP, *Trans. Nonferr. Met. Soc. China*, 19(5) (2009) 1303-1311.
- [14] B.V. Patil, U. Chakkingal, T. P. Kumar, Influence of outer radius in equal channel angular pressing, *World Academy of Science Engineering and Technology*, 62 (2010) 714-720.
- [15] M. Ensafi, G. Faraji, H. Abdolvand, Cyclic extrusion compression angular pressing (CECAP) as a novel severe plastic deformation method for producing bulk ultrafine grained metals, *Materials Letters*, 197 (2017) 12-16.
- [16] S. Ahmadi, G. Faraji, V. Alimirzaloo, A. Donyavi, Microstructure and Mechanical Properties of AM60 Magnesium Alloy Processed by a New Severe Plastic Deformation Technique, *Metals and Materials International*, 27 (2021) 2957-2967.
- [17] K. Hajizadeh, B. Eghbali, K. Topolski, K.J. Kurzydowski, Ultra-fine grained bulk CP-Ti processed by multi-pass ECAP at warm deformation region, *Materials Chemistry and Physics*, 143 (3) (2014) 1032-1038.
- [18] T. Altan, Cold and Hot Forging, *American Society for Metals*, 50-53 (2004).
- [19] H. Ataei1, M. Shahbaz, H. S. Kim, N. Pardis, Numerical Analysis of Plastic Strain Inhomogeneity in Rectangular Vortex Extrusion (RVE) Process, *Iranian Journal of Materials Forming*, 8(3) (2021) 46-52.
- [20] M. Shahbaz, N. Pardis, J. G. Kim, R. Ebrahimi, H. S. Kim, Experimental and finite element analyses of plastic deformation behavior in vortex extrusion, *Materials Science and Engineering A*, 674 (2016) 472-47.
- [21] Y. Iwashashi, J. T. Wang, Z. Horita, M. Nemoto, T. G. Langdon, Principle of equal channel angular pressing for the processing of ultra-fine-grained materials, *Scripta Materialia*, 35 (1996) 143-146.
- [22] Q. Ge, D. Dellasega, A. G. Demir, M. Vedani, The processing of ultrafine-grained Mg tube for biodegradable stents, *Acta Biomaterialia*, 9 (2013) 8604-8610.